Astronomy & Astrophysics

SCG0018-4854: a young and dynamic compact group[⋆]

I. Kinematical analyses

V. Presotto[1,2], A. Iovino[2], E. Pompei[3], and S. Temporin[4]

[1] Universitá degli Studi dell'Insubria, via Valleggio 11, 22100 Como, Italy
  e-mail: valentina.presotto@brera.inaf.it
[2] INAF - Osservatorio Astronomico di Brera via Brera 28, 20122 Milan, Italy
[3] European Southern Observatory (ESO) Alonso de Cordova 3107, Santiago, Chile
[4] Institut für Astro- und Teilchenphysik, Universität Innsbruck, Technikerstrasse 25, 6020 Innsbruck, Austria

ABSTRACT

Aims. It has been widely recognized that processes taking place inside group environment could be important drivers of galaxy evolution. Compact groups of galaxies in particular are excellent laboratories for studying galaxy interactions and their effects on the evolution of galaxies due to their high density and low velocity dispersion. SCG0018-4854 is a remarkably high galaxy density and low velocity dispersion group with evidence of a recent interaction. It has been detected and analyzed at different wavelengths, but its kinematics have never been studied in detail.
Methods. We obtained VLT FORS2 optical observations and present spectroscopic and photometric evidence to illustrate how dramatically galaxy interactions have affected each of the four group member galaxies.
Results. For each galaxy, we detected peculiar kinematics and evidence of recent star formation. In particular, the gas and stellar radial velocity curves of two galaxies are irregular with a level of asymmetry similar to that of other interacting galaxies. We discovered a bar inside NGC 92 thereby revising a previous morphological classification, and we obtained spectroscopic confirmation of the galactic-scale outflow within NGC 89.
Conclusions. The peculiar kinematics and dynamical considerations provide a rough estimate of the age of the latest interaction of $\tau \approx 0.2-0.7$ Gyr, suggesting that SCG0018-4854 is a young and dynamical group.

Key words. galaxies: clusters: individual: SCG 0018-4854 – galaxies: interactions – galaxies: kinematics and dynamics

1. Introduction

Compact groups (CGs) are among the smallest and densest systems of galaxies in the universe, and they are characterized by low velocity dispersions of the order of ≈ 200 km s^{-1} (Hickson et al. 1992). This is why they are excellent laboratories for studying galaxy interactions and their effects on the evolution of galaxies. Rubin et al. (1991) showed that 30% of spiral galaxies in CGs have distorted rotation curves and another 30% irregular velocity patterns indicating that tidal interactions are frequent and persist in CGs. Mendes de Oliveira & Hickson (1994) demonstrated that 43% of the galaxies in their compact group sample exhibit morphological and/or kinematical distortions indicative of interactions and/or mergers. Since these pioneering studies, it has been clear that interactions play an important role in the evolution of groups. According to current dynamical models, galaxies belonging to groups should interact violently and merge on a relatively short timescale (Sulentic 1987; Barnes 1985; Governato et al. 1996). Yet, strong mergers in CGs are rare (Mendes de Oliveira & Hickson 1994) and much effort has been made to establish the origin and fate of these systems. Coziol & Plauchu-Frayn (2007) showed that galaxies in compact groups are more likely to merge under dry conditions, after they

have lost most of their gas in interactions with galaxies. This hypothesis is corroborated by HI studies: Verdes-Montenegro et al. (2001) detected perturbed distributions of neutral hydrogen in CGs. These results indicate that the evolution of CGs is mainly dominated by galaxy interactions, continuous tidal stripping, and/or gas heating.

It is therefore interesting to reconstruct the evolution and the interaction history of a CG by studying the properties of its galaxy members and comparing them with the group properties as a whole. Kinematical and dynamical information are fundamental in separating between different interaction histories. Mendes de Oliveira et al. (1998) defined some kinematic indicators to distinguish between merging and interaction, such as the misalignment between the kinematic and photometric axis of gas and stellar components, double gas components, warping, and other peculiarities. However, open questions remain about how many interactions take place and how strong and frequent they are.

In this work, we focus on SCG0018-4854, a spiral-only compact group characterized by an extremely dense environment in which member galaxies have clearly interacted.

The plan of the article is the following. In Sect. 2, we present the characteristics of SCG0018-4854. In Sect. 3, we describe our observations and the reduction process. In Sect. 4, we explain the methods used for our analysis. The results are presented in

---

Table 1. SCG0018-4854 galaxy properties.

Galaxy	RA (J2000.0)	Dec (J2000.0)	V (km s^{-1})	Morphology	Activity	Notes
NGC 92	00:21:32	–48:37:29	3378 ± 10	SAa pec	SBG	tidal tail double nucleus?[1]
NGC 89	00:21:24	–48:39:55	3287 ± 10	SB0/a pec	Sy2	Hα galactic-scale extra-planar features[2] no HI detection[3]
NGC 87	00:21:14	–48:37:42	3415 ± 23	Irr	SFG	–
NGC 88	00:21:22	–48:38:25	3439 ± 19	SBab pec	LINER	–

Notes. RA and Dec data are taken from NASA/IPAC Extragalactic Database, while morphology and activity are taken from Pompei et al. (2007). **References.** (1) Danks & Alcaino (1981), (2) Temporin et al. (2005), and (3) Pompei et al. (2007).

Sect. 5, followed, in Sect. 6, by a short discussion and our conclusions in Sect. 7.

2. SCG0018-4854

SCG0018-4854 is an extremely compact group of four late-type galaxies: NGC 92, NGC 89, NGC 87 and NGC 88. It was originally listed in Rose's catalogue (Rose 1977) and is part of the Southern Compact Group catalogue (Iovino 2000). It is located at $v \approx 3240$ km s^{-1}, which means that $D \approx 45\ h_{70}$ Mpc, adopting $h_{70} = H_0/70$ km s^{-1} Mpc^{-1}. All galaxy members are within a projected distance of $\approx 1'.6$ from the center of the group, where $1''$ corresponds to 225 pc. A possible fifth member, ESO198-G013, is located at a distance of $\sim 15'$ in the E direction. Furthermore, SCG0018-4854 has a remarkably low velocity dispersion, ≈ 120 km s^{-1} and high density, 4.88 gal Mpc^{-3} on a log scale. Diffuse HI and X-ray emission have been detected confirming its bound nature (see Pompei et al. 2007; Trinchieri et al. 2008). The former data uncover a common HI envelope and a possible bridge between two galaxies, NGC 92 and NGC 88; according to Verdes-Montenegro et al. (2001), this HI distribution is typical of groups in phase 3b, i.e., with HI stripped from the galaxies and distributed in the common potential or in tidal tails. X-ray observation have detected a hot intergalactic medium, $kT \approx 0.2$ keV, in which the galaxies are embedded. The presence of both a warm and hot intergalactic diffuse medium is important not only as evidence of the gravitationally bound nature of SCG0018-4854, but also as proof of the galaxy interaction, even though it alone cannot explain the tidal structures. All four close members have a disturbed morphology, a late-type appearance, and intense star formation activity, as illustrated by early spectroscopic data (Coziol et al. 2000). Here we list the main properties of each galaxy, while additional information can be found in Table 1:

- NGC 92 is a SAa pec starburst, also classified as a LINER by Coziol et al. (2000). It has a ring of star-forming regions close to its centre part and an extended tidal tail in the SE direction with many HII regions (Temporin et al. 2005). A peculiar extension in the tail direction is also detected in X-rays (Trinchieri et al. 2008). It has also been proposed to contain a double nucleus (Danks & Alcaino 1981). The galaxy has clearly undergone an interaction with one or several group members;
- NGC 89 is a SB0/a pec that has a Sy2 nucleus and Hα-emitting extra-planar features with a filamentary structure on both sides of the disk, including a ~ 4 kpc-long filament with a jet-like structure extending in the NE direction (Temporin et al. 2005). It also has a ring of star-forming

regions around the nucleus. Interestingly, NGC 89 is the only galaxy of the group that was not detected in HI (Pompei et al. 2007). It has probably lost its neutral gas after interacting with other group members and the IGM;
- NGC 88 is the third spiral, SBab pec, of the group with a LINER nucleus. It forms an HI bridge with NGC 92 (Pompei et al. 2007);
- NGC 87 is a nearly face-on irregular galaxy, based on its axis ratio. It has many distinct regions of intense star formation.

All of these properties ensure that SCG0018-4854 is one of the few spiral-only and most active compact groups. It can be considered to be the southern counterpart of HCG16, the most active group of all Hickson compact groups. This group is located at a similar redshift and consist of four peculiar late-type galaxies, as described by Hickson (1982), another three members since being added (Ribeiro et al. 1996). It has been detected in both HI and X-ray data, which detected an intragroup medium (Verdes-Montenegro et al. 2001; Belsole et al. 2003). All galaxy member exhibit signs of interaction, such as tails and double nuclei, and different activities ranging from starburst to AGNs (de Carvalho & Coziol 1999). The interaction also affected the velocity field of each galaxy, as shown by Mendes de Oliveira et al. (1998) who detected peculiar kinematics.

SCG0018-4854 has been detected and analyzed at different wavelengths, but its kinematics has never been studied in detail. In this paper we present the first results of a kinematical analysis of galaxies in this group and we compare the member galaxy properties with those in HCG16. In a forthcoming paper (Temporin et al. in preparation), we will analyze in detail the photometric and morphological properties of each galaxy of SCG0018-4854, focusing on the likely age of the stellar populations and their correlation with morphological structures.

3. Observation and data reduction

The spectroscopic data were obtained with the FORS2 spectrograph at the VLT-UT1, (Appenzeller et al. 1998) during an observing run in September 2001. The detector was a 2048 × 2048 px CCD with a scale of 0.201$''$ px^{-1} (we used the standard resolution collimator). We acquired spectra using the spectroscopic mask mode (MXU), which enables a mask with slits of different length, width, shape, and inclination to be created according to the observational demands. We designed two different masks, one for all spectra along the major axis and another for all spectra along the minor axis. We were unable to observe the major axis of NGC 88 because of overlaps between the slits in the same mask. We needed to use two different slits to cover the entire galaxy extent of NGC 92 (both axis) and NGC 89

Table 2. Slit properties of the mask along the major axis.

Gal slit	Width (″)	Length (″)	i (deg)	PA (deg)	λ coverage (Å)
NGC 92	1	2×39.8	0	−29	4845–5895
NGC 89	1	2×35	−18	−47	4530–5585
NGC 87	1	30.5	39	10	4450–5490

Notes. i = inclination angle with respect to the dispersion axis, PA = position angle with respect to the N direction.

(major axis). The data consist of four exposures of 2699 s for both masks, covering the major and the minor axis. All slits are 1″-wide and have different lengths, positions and inclinations with respect to the dispersion axis. We used the GRISM-1400V with a dispersion of 20.8 Å mm^{-1}, corresponding to 0.49 Å px^{-1}. The grism peak is at 5200 Å and the spectral coverage of each object spectra is ≈1000 Å in the 4500–5900 Å wavelength range according to the slit position with respect to the center of the CCD. Figure 1 and Tables 2 and 3 show the slit positions and properties. A set of He-Cd-Hg-Ne lamp spectra were obtained for each observing night. The average seeing was about 0.7″ throughout our exposures. The individual frames were pre-reduced (e.g., bias subtraction, flat-field correction, etc.) using standard IRAF[1] image processing packages. The wavelength calibration was performed using the IRAF twodspec.longslit package. Our spectra have different inclination angles with respect to the dispersion axis. To rectify them we adapted the parameters of the task reidentify forcing it to identify and calibrate each lamp emission-line row by row. We verified our final wavelength solution using available skylines row by row. We adopt the rms of the $\lambda 5577$ Å skyline centroid distribution, ≈0.1 Å, to be the calibration accuracy. The wavelength coverage for NGC 87 does not include any strong skyline so we verified the calibration directly on lamp spectra. We obtained the same accuracy as above. We found a systematic offset of ≈0.5 Å in the calibration of all spectra along the major axis, which is probably caused by instrument flexure (see Gallart et al. 2001). The final spectral resolution was measured to be 2.25 Å (*FWHM* of $\lambda 5577$ skyline), equivalent to a velocity of $\sigma \approx 51$ km s^{-1}. The sky subtraction was performed using a narrow region, ≈10 px, at both edges of the slit where there was minimal galaxy contamination. Unfortunately, we could not remove the sky from the spectrum along the major axis of NGC 87 because the galaxy covers the entire length of the slit and a longer slit would have caused problems of overlap with the others. Our attempts to reproduce the sky level reliably failed, so we preferred not to subtract it. We extracted 1D spectra by binning each 2D spectrum along the spatial direction to ensure a signal-to-noise ratio $(S/N) \geqq 6$ at all radii. It should be noted that in the central pixels, we have a $S/N \geqq 100$, and for this high S/N data we just take into account the seeing when binning spectra to ensure that the data are uncorrelated spatially.

4. Analysis method

4.1. Radial velocity curves

Stellar kinematics was derived using the cross-correlation technique (Tonry & Davis 1979) with the IRAF RVSAO package.
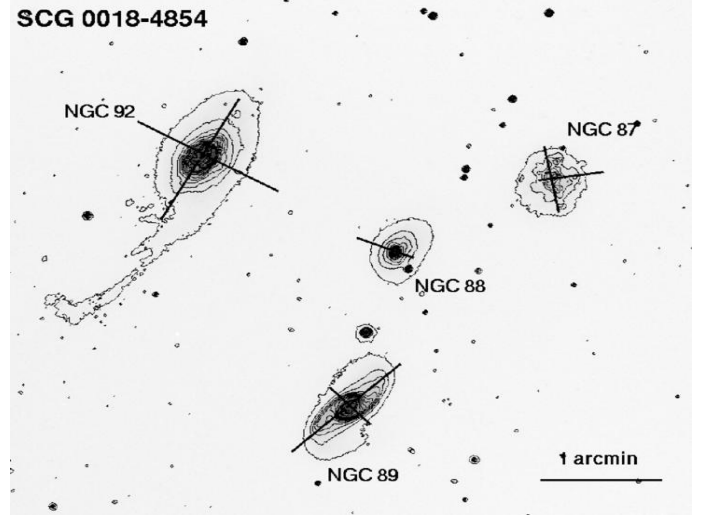
Fig. 1. *R*-band image of SCG0018-4854 with the slits and isointensity contours overlayed. North is up and east to the left.

Table 3. Slit properties of the mask along the minor axis.

Slit	Width (″)	Length (″)	i (deg)	PA (deg)	λ coverage (Å)
NGC 92	1	2×39.9	0	60	4620–5650
NGC 89	1	28	−18	42	4850–5890
NGC 87	1	25	38.7	−81	4450–5490
NGC 88	1	30	7.5	67	4620–5650

Notes. i = inclination angle with respect to the dispersion axis, PA = position angle with respect to the N direction.

The cross-correlation was performed for a wavelength range of ≈900 Å about the main absorption features of the Mg line triplet ($\lambda\lambda 5164, 5173, 5184$ Å). We decided to use the nuclear spectra of each galaxy as a template, thereby minimizing problems caused by template mismatch. In this way, we derived the relative velocities at various distances from the nucleus and so constructed the stellar radial velocity curve. Errorbars were derived by adding in quadrature the contributions from photon statistics, CCD read-out noise, and calibration accuracy. We notice that the stellar errorbars are always larger than those of the gas ones because the stellar cross-correlation was performed in a wavelength range with few absorption lines. Furthermore, those present in the spectra are quite weak, causing the fit to have a large error.

To obtain the systemic velocity of each galaxy, we performed a second cross-correlation with a radial velocity standard star extracted from the ESO archive. We used HD 36 003, a K star, using an observing set-up that matches that of our data well. We assumed that the photometric center coincides with the dynamical one, and we defined the systemic velocity of each galaxy to be that obtained by a cross-correlation between the standard star and the center of the galaxy along the major axis. All quoted velocities are corrected to the heliocentric reference system.

As already discussed, we could not measure the stellar kinematics of NGC 87 along the major axis because of the presence of sky contamination. We therefore decided to use the value of velocity measured at the center of the galaxy in the minor axis spectrum as the systemic velocity.

The ionized gas kinematics were measured by applaing a Gaussian fit to the main emission lines present in the spectra

(Hβ, [OIII] λλ4959, 5007) using the IRAF onedspec.splot task. We derived the errors by adding in quadrature both the calibration accuracy and the formal errors given as output by the fitting routine.

We discovered multiple components in the emission line profile of NGC 92 and NGC 89. In the case of NGC 92, we found two components that we used the deblending function of SPLOT to separate, obtaining errorbars as described above. For NGC 89, the emission profile is quite complex, and may indeed represent three or more overlapping components (see Sect. 5.2). We therefore used the task NGAUSSFIT to attempt to deblend them. In this case, the errorbars of gas velocities are found to be the sum in quadrature of uncertainties from four different sources: (1) the finite slit width, which introduces an uncertainty of 1.2 Å; (2) the rms of the peak centroid for different fitting solutions that were obtained by perturbing the initial centroid guesses, which ranges between 0.01 and 0.5; Å according to the component; (3) the error in the best-fit solution, which ranges between 0.001 and 0.5 Å; and (4) the calibration accuracy of 0.1 Å. All of these terms infer a velocity error that ranges between 65 and 85 km s^{-1} according to the component.

4.2. Asymmetry parameter

We wished to detect any sign of interactions and how they had affected the kinematical properties of the galaxies. As we have said, most galaxies in groups have irregular or anomalous rotation curves so we attempted to quantify any asymmetry. As an indicator we used the asymmetry parameter, AP, described by Dale et al. (2001)

$$ AP = \sum \frac{\|V(R)\| - |V(-R)|\|}{\sqrt{\sigma^2(R) + \sigma^2(-R)}} \times \left[\frac{1}{2} \sum \frac{\|V(R)\| + |V(-R)|\|}{\sqrt{\sigma^2(R) + \sigma^2(-R)}} \right]^{-1}. $$

This parameter takes into account the different behaviors of the kinematically folded approaching and receding halves, so quantifies any possible asymmetries in the observed rotation curves. The error in AP was estimated as follows for each velocity measurement, $V(R_i)$, we generated a normal velocity distribution centred on $V(R_i)$ with a dispersion σ equal to the errorbar $\sigma(R_i)$ of $V(R_i)$ and selected a random value, $V_{new}(R_i)$. We then estimated the new AP using $V_{new}(R_i)$ and $\sigma(R_i)$. We repeated this procedure in a $N = 10\,000$ cycle and then adopted as the AP error the rms of the resulting AP distribution, which resembles a normal distribution.

5. Results

5.1. Kinematics of NGC 92

In Fig. 2, we present the stellar (filled circles) and gas (open circles) radial velocity curves of NGC 92 along both the major (panel a) and the minor (panel b) axes. The kinematics along the major axis has two important features: i) at each radius, the gas rotates faster than the stars, the former reaching a maximal velocity of $V_{gas} \approx 200{-}220$ km s^{-1}, and the latter a maximum of $V_* \approx 140$ km s^{-1}; ii) While the stars exhibit a regular radial velocity curve, the gas radial velocity curve is asymmetric with respect to the center of the galaxy. There is a steep rise in V_{gas} up to 220 km s^{-1} within 1 kpc in the NW direction, whereas on the other side the gas velocity reaches only 160 km s^{-1}. We discover that the gas also rotates along the minor axis (see Fig. 2).

The emission-line profiles of Hβ and [OIII] λλ4959, 5007 along the minor axis detect a secondary component in addition
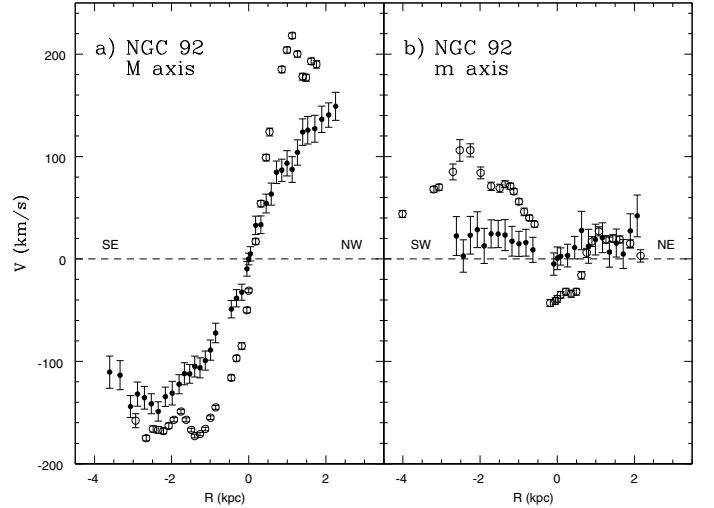

Fig. 2. Gas (open circles) and stellar (filled circles) kinematics along the major panel **a)** and minor panel **b)** axis of NGC 92.
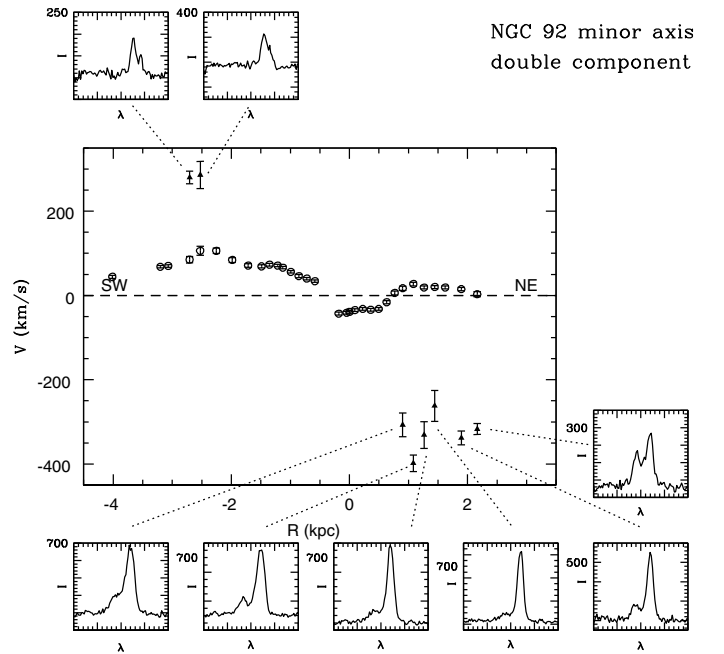
Fig. 3. Position-velocity diagram with both the main (open circles) and the second (filled triangles) component of gas along the minor axis of NGC 92. Smaller panels show the zoom of 1D spectra in the range 5040–5080 Å containing the [OIII] emission line at each position where we were able to measure both components.

to the main one. In Fig. 3, we show the position-velocity diagram with both the main (open circles) and the second (filled triangles) component of gas along the minor axis of NGC 92. The smaller panels show the zoom of 1D spectra in the range 5040–5080 Å of the [OIII] emission line at each position where we were able to measure both components. Close to the nucleus, an asymmetry in the profile is indicative of a second component, and at ~1 kpc from the nucleus, an additional second peak is clearly evident, as shown in the smaller panels of Fig. 3. At distances greater than 2.5 kpc, we do not detect the second component anymore.

The velocity gap between the components is $\Delta V \approx 200$ km s^{-1} in the SW direction, whereas it reaches $\Delta V \approx 350$ km s^{-1} in the NE direction. There are two possible explanations of this double component: we are either detecting infalling
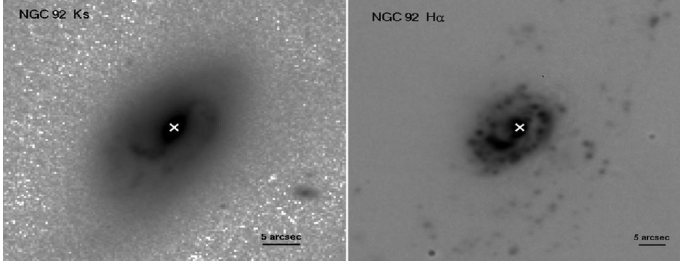
Fig. 4. *K*s-band (*left*) and continuum-subtracted Hα + [NII] (*right*) images of NGC 92. North is up and east to the left. The bar is clearly visible in the *K*s image. Despite the different pixel scales of these images, it is clear that the Hα bright knot to the SE is the elbow of a spiral arm pointing towards the observer.

gas with extra-planar motions (Fraternali & Binney 2008) or the two components trace the well known eight-shape caused by a bar (Kuijken & Merrifield 1995). To understand which of the two proposed explanations is more likely, we inspected the *K*s-band and the continuum-subtracted Hα + [NII] images[2] of NGC 92 (hereafter Hα refers to Hα + [NII]). The *K*s-band image was obtained with SOFI at NTT and has a scale of $0.288''\,\mathrm{px}^{-1}$, whereas the Hα image was obtained with FORS2 and has a scale of $0.1''\,\mathrm{px}^{-1}$. These data will be presented and analyzed in detail in a forthcoming paper (Temporin et al. in preparation). Here we just report a few morphological details of the inner regions of NGC 92 that are particularly useful to our interpretation of the kinematic features. The two images are shown in Fig. 4. The *K*s image clearly shows a bar, thus corroborating the hypothesis that the second gas component along the minor axis is related to a bar. From the comparison with the Hα image, it also appears to be clear that the Hα bright knot to the SE of the galaxy nucleus, thought to be a secondary nucleus, is the elbow of an inner proceeding spiral arm. In Sect. 6, we explore and discuss the implications of the presence of a bar for NGC 92.

In Fig. 5, we show the folding of the stellar (panel a) and the gas (panel b) radial velocity curves and their *AP*. The behavior of the stars looks quite regular, whereas the gas is far more perturbed. We obtain *AP* values of $11\% \pm 4\%$ and $23\% \pm 1\%$ for the stars and the gas, respectively. Pedrosa et al. (2008) used simulations to analyze the *AP* of interacting and unperturbed galaxies in CGs and compare this with observations. They found that *AP* ≈ 13–36% for the former and *AP* ≈ 5–7% for the latter. These two ranges of values are in good agreement with our estimates for the observed velocity curves of the stars and the gas, respectively. Therefore, the stars of NGC 92 are unperturbed or only slightly perturbed, while the gas *AP* agrees with values obtained for other perturbed galaxies in groups. A mismatch between the two sides of the rotation curve was also independently found by Torres-Flores et al. (2009) based on Fabry-Perot data. They also found signs of secondary kinematical components and a possible signature of non-circular motions. We refer to Sect. 6 for a detailed discussion.

Additional emission lines are detected in both the nucleus of NGC 92 and the surrounding regions. These are HeI λλ 5015.68, 5875.6, [NI] λλ5198.5, 5200.7, and [NII] λ5754.6. Some of these lines require a sufficiently hard ionizing radiation source (Osterbrock & Ferland 2006) and, therefore, are normally found

---

[2] The [NII]/Hα emission line ratios evaluated within several regions of the galaxy by means of lower resolution spectra (not presented in this paper) together with the shape of the narrow-band filter transmission curve show that the [NII] emission lines contribute roughly 11.5% of the flux in the narrow-band image.
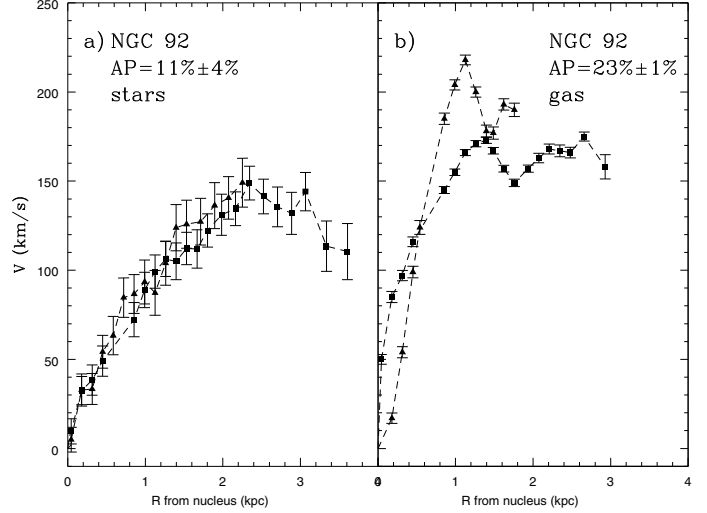

Fig. 5. Folding of the stellar panel **a)** and the gas panel **b)** radial velocity curve of NGC 92. Triangles are used to represent the receding side, in NW direction and squares the proceeding side, in SE direction. The *AP* values obtained for the stars and the gas are indicated.

in regions photoionized by AGN radiation, or in regions of strong and recent star formation, although most of them are generally difficult to detect because of their weakness. It is interesting to note that the (usually very weak) HeI λ 5015.68 emission-line was detected only in correspondence with the elbow of the inner spiral arm, where additional data (not presented here) provides evidence of the explosion of a supernova in the year 1999 (Temporin et al., in preparation). The [NII] λ5754.6 line – which is a well known electronic temperature indicator for the low ionization zones of gaseous nebulae, when combined with the more easily detectable [NII] λλ 6548, 6583 emission lines – is visible in both the same spectrum and the nuclear one. Finally, the [NI] doublet is detected in the nucleus and in all spectra out to 1.4 kpc NW and 2.1 kpc SE of the nucleus along the major axis. Vaona et al. (in preparation), in a statistical study of the NLR of Sy2 galaxies extracted from the SDSS, find that the [NI] λλ5198.5, 5200.7 doublet is detected in 8% of their sample (169 out of 2153 galaxies) and has a median ratio to Hβ of $\sim 0.14 \pm 0.06$. This value is consistent with what we observe in the nuclear region of NGC 92, which is classified as a LINER. Further out, the [NI]/Hβ ratio assumes values of the order of a few 10^{-2}, similar to those observed for HII regions in other LINER galaxies (e.g., Díaz et al. 2000). These [NI] lines are even observed in the presence of relatively weak radiation fields, as in the partially ionized zones of the Orion Nebula, and fluorescence is thought to play an important role in their excitation (Bautista 1999).

5.2. Kinematics of NGC 89

In Fig. 6, we present the stellar (filled circles) and gas (open circles) radial velocity curves of NGC 89 along both the major (panel a) and the minor (panel b) axis. Along the major axis, we can measure velocities only out to 2 kpc from the nucleus and both the gas and the stars reach a maximum $V \approx 100\,\mathrm{km\,s}^{-1}$. In the inner regions, $R < 1$ kpc, gas and stars have similar kinematics, while further out the gas has a slightly less regular pattern. In particular, we note that major discrepancies occur at $R \approx 1$ kpc in the NW direction. The gas kinematics is also perturbed along the minor axis: in the SW direction, the gas velocity starts to
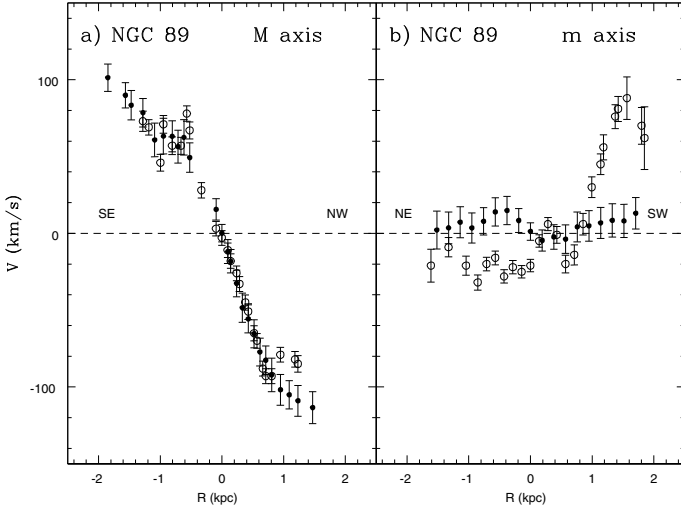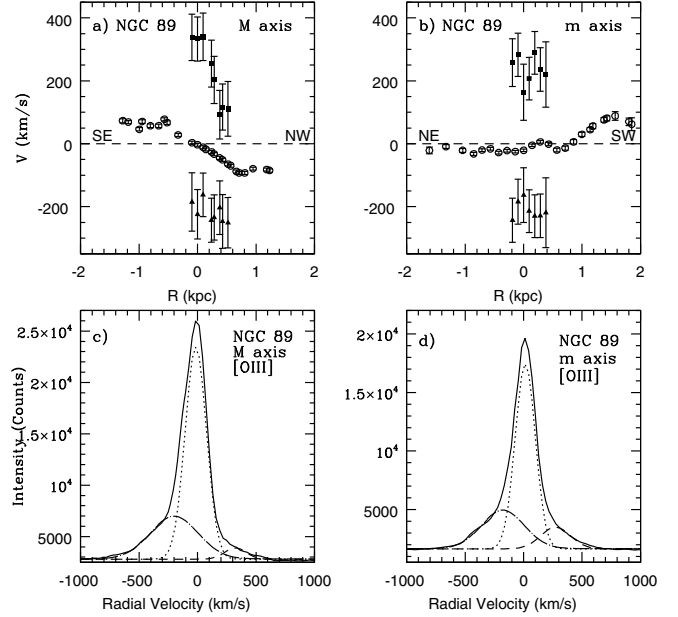
Fig. 6. Gas (open circles) and stellar (filled circles) kinematics along the major panel **a)** and the minor panel **b)** axis of NGC 89.
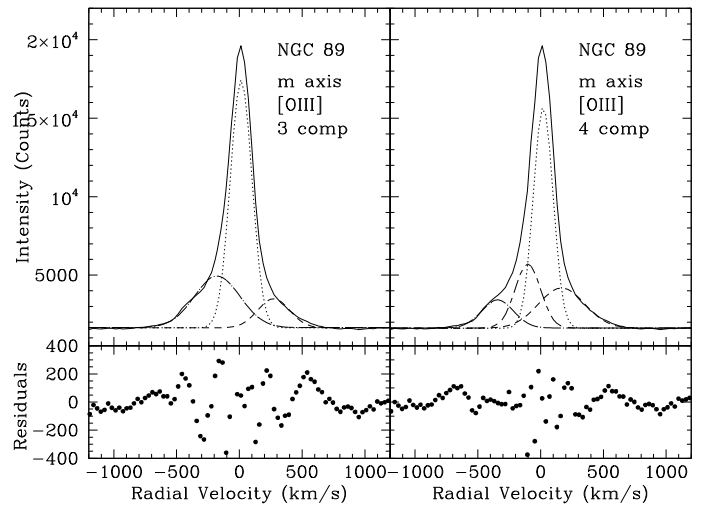

Fig. 7. NGC 89: position-velocity diagram along the major panel **a)** and the minor panel **b)** axis and the [OIII] emission-line profile obtained by summing 6 pixels (1″2) around the nucleus along the major panel **c)** and the minor panel **d)** axis as a function of velocity with respect to galaxy systemic velocity. We fit the profile with a combination of three Gaussians: the main component (open circles and dotted line), the blue-shifted component (filled triangles and dot-dashed line), and the red-shifted one (filled squares and dashed line).

increase at ≈ 1 kpc and reaches $V \approx 90$ km s^{-1} at 1.5 kpc. We suggest that the gas kinematics is affected by both the central AGN and the Hα-emitting extraplanar gas (see Sect. 2).

We observe that the emission-line profile of [OIII] is asymmetric and irregular because of the presence of multiple components, at least three, in the nuclear region. This kind of profile is typically observed in the narrow-line regions (NLR) of Sy2 galaxies. It is understood that photoionization and shocks play a dominant role in modifying the physical conditions of the gas (Dopita et al. 2002; Kraemer & Crenshaw 2000; Veilleux et al. 2005), although the dynamics of the gas in the NLR is less certain. The presence of blue-shifts and red-shifts on either side of the nucleus indicates that rotation alone cannot explain the observed radial velocities. Emission-line profiles can be reproduced by different kinematic models such as infall, outflow, rotation (Osterbrock & Mathews 1986; Veilleux 1991). The general idea is that radial outflows play an important role.

The top panels of Fig. 7 show the position-velocity diagrams along the major (panel a) and the minor (panel b) axis for the main gaseous component (open circles), the [OIII] blue-shifted component (filled triangles), and the [OIII] red-shifted one (filled squares). We observe non-circular motions of the gas of high velocity, $V \approx \pm 200$ km s^{-1}. In particular, the red-shifted component along the major axis has a regular pattern of high velocity within 150 pc of the nucleus and then decelerates as we go farther away, 500 pc, in analogy to other cases of Sy2 NLR kinematics (see Das et al. 2006, and references therein). The multiple components can be more clearly seen in the spectral extractions around the nucleus. The bottom panels of Fig. 7 show the [OIII] emission-line profile obtained by summing 6 pixels (1″2) around the nucleus along the major (panel c) and the minor (panel d) axis as a function of velocity with respect to the systemic velocity of the galaxy. We fit the profile with a combination of three Gaussians: the main component (dotted line), the blue-shifted component (dot-dashed line), and the red-shifted one (dashed line). The blue-shifted component along the minor axis is unable to fit two different bumps in the [OIII] emission-line profile and a fourth component is probably needed to reproduce the [OIII] profile. We are able to perform the fit with four components in a satisfactory way only at the galaxy center. In Fig. 8, we compare the fit using three Gaussians (left) with the fit with four Gaussians (right). Residuals of the fit are shown in the bottom

Fig. 8. Multiple component of the [OIII] emission-line profile along the minor axis of NGC 89. We compare the fits to the profile using a combination of three (*left*) or four (*right*) Gaussians. *In the bottom panels*, we show residuals for both cases. The choice of four Gaussians, the main component (dotted line), two blue-shifted components (dot-dashed and short-long dashed line), and the red-shifted one (dashed line) provide more reliable results.

panel in both cases. The choice of four Gaussians, the main component (dotted line), two blue-shifted components (dot-dashed and short-long dashed line), and the red-shifted one (dashed line) provide superior results, $\chi^2 \approx 1.7$, to that of three components, $\chi^2 \approx 2.3$. The former residuals show closer agreement with the rms of the continuum as measured in two regions of 40 pixels at the edges of the emission-line profile. Although increasing the number of free parameters would provide a smaller χ^2, we
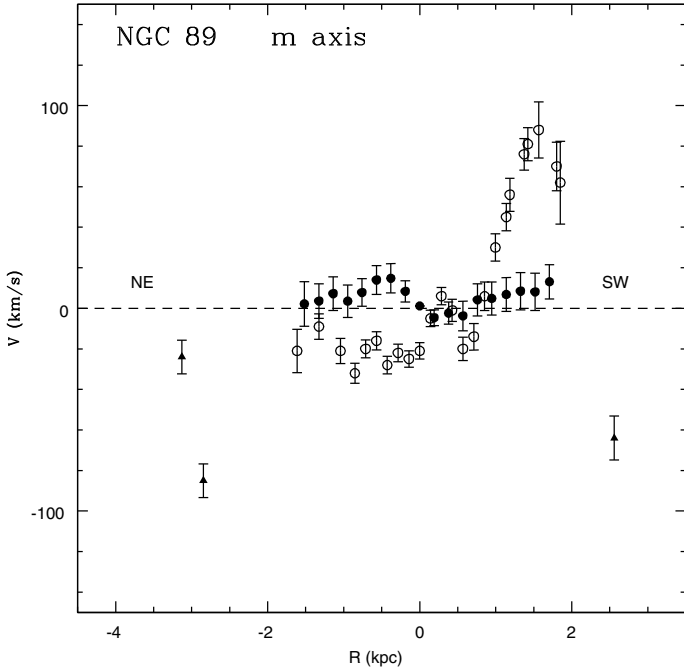
Fig. 9. Kinematics along the minor axis of NGC 89. Measured radial velocities of the primary gas component (open circles), the secondary gas component (filled triangles), and the stars (filled circles) are plotted. The kinematics of the secondary gas component is consistent with the presence of an outflow.

Fig. 10. Folding of the stellar panel **a)** and gas panel **b)** radial velocity curve of NGC 89. Triangles are used for the receding side in the SE direction, and squares for the approaching side in the NW direction. The values of the *AP* for the gas and the stars are indicated.
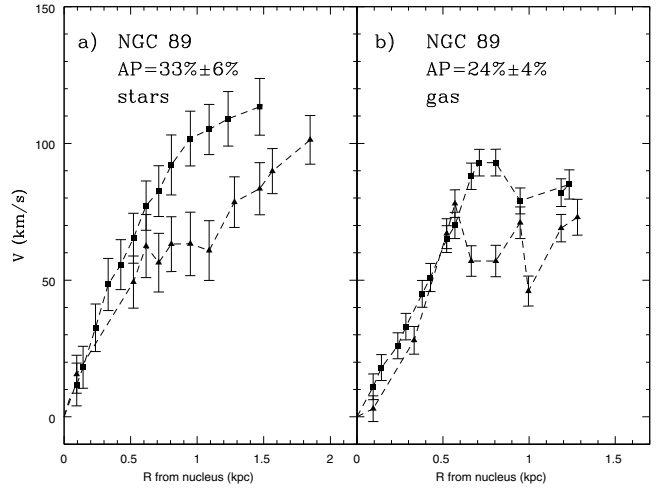
should keep in mind that it also leads to a degeneracy in the solutions. It is then difficult to establish which is the most reliable, and 3D spectroscopy of longer integration time could help us to assess whether a fourth component is present.

However, we note that this fourth component survives few pc away from the nucleus only in NE direction, which is the same direction as the galactic-scale Hα brightest filament. We cannot exclude that these two features are somehow linked to each other. The slit along the minor axis intercepts the jet-like filament at three different points. We are therefore able to probe it spectroscopically and compare its kinematics with that of the adjacent gas.

In Fig. 9, we plot the measured kinematics of the additional gas components (filled triangles) with the gas (open circles) and stellar (filled circles) radial velocity curves. The kinematics of the extraplanar gas is clearly decoupled from the disk gas kinematics. In the SW direction, the velocity of this gas component appears to an opposite sense to that of the disk gas. In the opposite direction, we have two measurement and there is a possible indication that the secondary gas component slows down as we go farther away from the center of the galaxy. The decoupled kinematics of the secondary gas component is compatible with the presence of an outflow. We discuss this possible interpretation in Sect. 6.3.

Once again, we estimated the asymmetry parameter. In Fig. 10, we show the folded stellar (panel a) and gas (panel b) radial velocity curves and the relative *AP*. We measure an *AP* value of 33% ± 6% and 24% ± 4% for the stars and the gas, respectively. These large values, as already mentioned in Sect. 5.1, are typical of strongly perturbed galaxies. We refer to Sect. 6 for a more detailed discussion.

This galaxy also exhibits many emission lines in its nuclear spectrum, in particular HeII λ4685.75. This emission line can be observed in gas photoionized by the hard radiation field of an active galactic nucleus or be produced by the wind of Wolf-Rayet (W-R) stars (e.g., Crowther 2007), thus indicating that a recent burst of massive star formation may have occurred (Schaerer & Vacca 1998). In W-R galaxies this emission line is usually broad (although often accompanied by a narrow nebular component that is too weak relatively to be reliably detected) and forms the so-called "W-R bump" in the spectrum together with other strong emission lines (e.g., of CIII, CIV, and NIII) in the wavelength range λ4650–4690 (Schaerer & Vacca 1998, and references therein). Since the emission line that we observe is narrow, is not accompanied by a W-R bump and other typical features of W-R galaxies, and is visible only in the nuclear spectrum of NGC 89, we conclude that it is unlikely to be indicative of Wolf-Rayet stars, but rather be the nebular emission produced by the ionizing radiation of the central AGN.

5.3. Kinematics of NGC 87 and NGC 88

We describe the kinematical properties of the two remaining group members: NGC 87 and NGC 88.

In Fig. 11, we present the stellar (filled circles) and gas (open circles) radial velocity curves of NGC 87 along the minor axis (panel b), while along the major axis (panel a) we show only that of the gas (open circles). Our lack of stellar kinematical data along the major axis is caused by problems in sky subtraction that made the use of XCSAO impossible (see Sect. 4). The gas shows a velocity gradient along both axes upon which peculiar motions are superimposed. These peculiar motions relate to different regions of emission in the irregular galaxy. In both cases, the velocity gradient is a regular trend with a significant velocity variation with respect to the errorbars and the velocity range of peculiar motions. Nevertheless, we cannot determine wheter if the velocity gradient is associated with either the whole galaxy or only a few regions, or if it represents a warp. The HI gas emission is more extended than the optical light and the emission looks asymmetric; the HI velocity field does not show any significant gradient, as it would for an almost face-on galaxy, except in the N/NE corner at approximately the same position where the velocity gradient measured in the optical exhibits the widest variation.
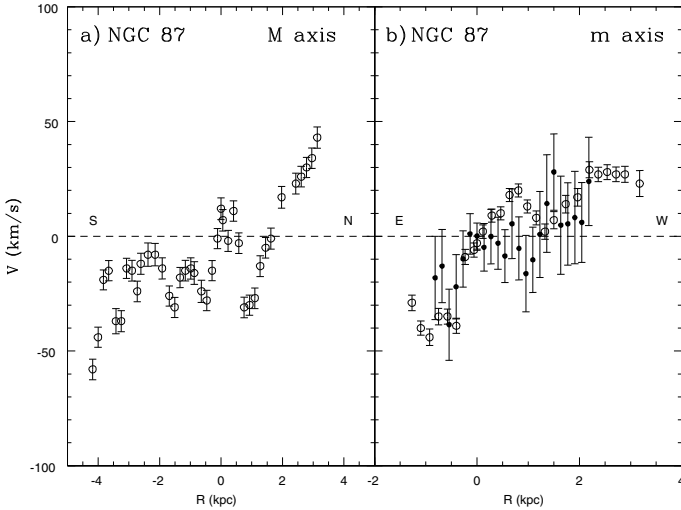
Fig. 11. Panel **a)** Gas (open circles) kinematics along the major axis of NGC 87. Panel **b)** Gas (open circles) and stellar (filled circles) kinematics along the minor axis of NGC 87.

Fig. 12. Gas (open circles) and stellar (filled circles) kinematics along the minor axis of NGC 88.

In Fig. 12, we show the stars (filled circles) and gas (open circles) kinematics along the minor axis of NGC 88. The gas shows a sinusoidal pattern that possibly indicates a regular rotation. Once again, the ionized gas moves on extra-planar orbits. This type of kinematics is common in galaxy bulges (Coccato et al. 2004) and could be generated by a triaxial bulge or a bar. Kinematical information along the major axis is needed to find out which hypothesis is more likely (Corsini et al. 2003).

6. Discussion

6.1. Kinematical effects of the interaction on galaxies involved

NGC 92 has clearly interacted with one or several group members as suggested by the extended tidal tail. We discuss the kinematical effects of this interaction and the most probable other interacting galaxy or galaxies.

The stellar radial velocity curve of NGC 92 is only moderately perturbed, whereas the gas has an asymmetric radial velocity curve. The receding side has a steeper rise than the approaching one. We note that the approaching side is in the direction of the tidal tail and we assume that the tail affects the gas kinematics by keeping velocities at an approximately constant value of $160\,km\,s^{-1}$. This is consistent with HI data: neutral hydrogen velocities show a continuous trend between the tidal tail and the approaching side of the galaxy disk, clearly suggesting a physical link between the gas, disk, and tail (Pompei et al. 2007). Arp 295 is a similar case of interacting galaxies with asymmetric rotation curves (Roche 2007). For Arp 295, the rotation curve also rises slowly and monotonically on the side pointing towards the tail and the companion, whereas on the other side it rises more steeply. Furthermore, interacting galaxies have been found to exhibit a correlation between the star-formation rate (SFR) and perturbed kinematics (Keel 1993). The SFR increases as the rotation curves become more asymmetric from normal to disturbed rotation curves. Therefore, we expect to detect enhanced star formation in NGC 92. Previous results of an Hα study of SCG0018-4854 found that the luminosity function of the HII regions of NGC 92 exhibits a considerable flattening at the high luminosity end (Temporin et al. 2005). NGC 89 and NGC 88 are likely to be interacting with NGC 92, and we have measured
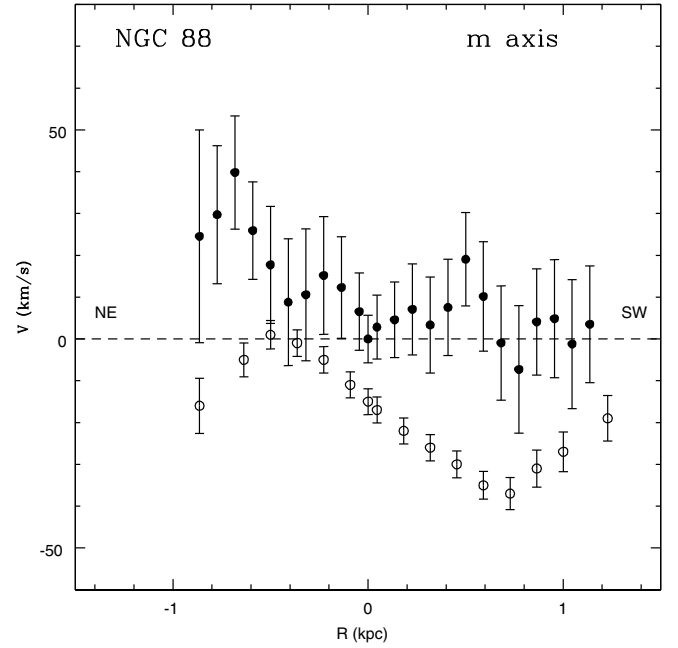
irregular radial velocity curves and peculiar kinematics for both galaxies.

NGC 89 has perturbed stellar and gas radial velocity curves, suggesting that it has interacted with other group members. Both the gas and stars have lower velocities on the receding side than the approaching one. This could be the result of different phenomena: (1) a disk warp, (2) streaming motions induced by an interaction, or a (3) combination of disk and spiral arm motions. Although currently unavailable for this galaxy, 3D spectroscopy would help us to distinguish among these possibilities. Anyway, it is interesting to note that neutral and molecular hydrogen studies of this galaxy support the hypothesis that NGC 89 has interacted in the past with other group members. NGC 89 has been completely stripped of its HI gas (Pompei et al. 2007) and CO observations show that it is also perturbed in its molecular gas distribution (Boselli et al. 1996). These facts suggest that also the perturbed kinematics of NGC 89 is a consequence of previous interactions, the most likely perturber being NGC 92.

NGC 88 shows a sinusoidal pattern of the gas velocities probably caused by a triaxial bulge or a nuclear bar. Both phenomena could be the result of an interaction. There is also an HI bridge between NGC 92 and NGC 88 (Pompei et al. 2007). Broad-band observations show a wide stellar tail extending from this galaxy towards the south-west (Temporin et al. in preparation).

The interaction process probably only partially involves NGC 87: we found velocity gradients along both axes which could be the result of a slight interaction with other members. A stronger encounter would probably disrupt galaxy more dramatically because of its irregular morphology and lower mass.

6.2. The interaction strength and history of SCG0018-4854 galaxies

The suggestion that NGC 92 contains a double nucleus (Danks & Alcaino 1981) could imply that this galaxy is a merger remnant. If this were the case, NGC 92 should have interacted violently

with a companion galaxy in the past. Our results show that even if the interaction has been strong, we can exclude the hypothesis of a merger for NGC 92. The discovery of the nuclear bar indeed rejected the hypothesis of a double nucleus. The comparison between Ks-band and Hα images shows that the bright knot is actually the elbow of the inner proceeding spiral arm that departs from the nuclear bar. Therefore, NGC 92 should have interacted more recently and less strongly than the presence of a double nucleus would suggest.

However, it is well known that structures such as bars and rings could arise from galaxy interactions (Lindblad 1961; Noguchi 1987; Gerin et al. 1990). A direct tidal interaction acts as a destabilizing agent, reducing the bar formation timescale and accelerating the growth of the bar. Hence, we cannot exclude that the nuclear bar of NGC 92 be a product of its interaction with other group members and the presence of the tidal tail strengthens this hypothesis. Future 3D-spectroscopy could help us to understand the origin of the bar, e.g., gas inflow could be an evidence of recent bar formation. Furthermore, a detailed study of the star formation along the bar could help us to state whether the bar is linked to the interaction or not.

We try to quantify the interaction strength by estimating the asymmetry parameter for the NGC 92 and NGC 89 radial velocity curves. Cluster galaxies have a mean AP of $12.6\% \pm 1.2\%$ (Dale et al. 2001), while, as we have already said, galaxies in groups have larger values. We measured AP values in the range 11–33%, which are in agreement with values of other perturbed and interacting galaxies in CGs. The gas is the first component to be affected by an interaction. The gas kinematics of both NGC 92 and NGC 89 have been strongly perturbed. In contrast, stellar kinematics are perturbed if the interaction has been violent. Therefore, since NGC 89 only shows perturbed stellar kinematics, we speculate that the interaction was stronger for this galaxy than for NGC 92. Furthermore, taking into account that NGC 89 is the only galaxy of the group depleted of HI we cannot exclude a more complicated interaction history for this galaxy. NGC 89 could have interacted with the other group members several times, NGC 92 being the latest one. Otherwise, NGC 89 may have joined the group only recently: the interaction with the group potential removed its gas before it interacted with NGC 92. Hydrodynamical simulations could help us to infer the more likely scenario. Some caution is necessary, since studies have shown that the appearance of distortions in rotation curves is strongly dependent on the viewing angle (Kronberger et al. 2006). In any case, there is a clear trend of increasing AP for interacting galaxies. Pedrosa et al. (2008) analyzed the evolution of AP in simulations of galaxy encounters with varying set-up. They showed that AP rises at the peri-passage by values of up to $\approx 20\%$ and it begins to decrease only after $0.7\,\mathrm{Gyr}\,h_{70}^{-1}$. In other words, AP could be used as a timer of recent interactions. Since SCG0018-4854 is a compact group, its galaxies are supposed to encounter each other many times during their lives. We attempt to determine the age of the latest interaction among the galaxies of this group by measuring the AP. Our estimated values of AP for the gas and stars of NGC 92 and NGC 89 are large and indicative of a recent interaction. Hence, NGC 92 and NGC 89 should have interacted within the past 0.7 Gyr. This is only an upper limit, since dynamical considerations on the tidal tail infer a more recent interaction. A rough estimate of the age of the latest interaction is given by $\tau_{\mathrm{tail}} \approx L_{\mathrm{tail}}/V_{\mathrm{flat}}$, where L_{tail} is the tail extent of $\approx 30\,\mathrm{kpc}$, and V_{flat} is the velocity at which rotation curves become flat. In the tail direction, V assumes an approximately constant value of $\approx 160\,\mathrm{km\,s^{-1}}$, which implies that $\tau_{\mathrm{tail}} \approx 190\,\mathrm{Myr}$.

The above considerations lead us to an estimated age of the latest interaction of $\approx 0.2\,\mathrm{Gyr} < \tau_{\mathrm{coll}} < 0.7\,\mathrm{Gyr}$, which is comparable with the crossing time of this group of $0.272\,\mathrm{Gyr}$ (Pompei et al. 2007). Additional constraints will be obtained by estimating of the age of the stellar populations by means of a detailed photometric analysis, which will be the subject of the already mentioned forthcoming paper.

6.3. A galactic-scale outflow in NGC 89

As mentioned in Sect. 2, the continuum-subtracted Hα image of NGC 89 shows the presence of ionised extra-planar gas (Temporin et al. 2005). This gas appears to be organised in a biconical structure departing from the central part of the disk and extending roughly perpendicularly to the disk plane on both sides of the disk. It has a filamentary structure and the prominent 4-kpc long jet-like structure is possibly just the brightest of these filaments. The origin and the nature of these Hα filaments cannot be fully established with the data presently available, but their geometry is consistent with them being a galactic-scale outflow. This outflow could be driven by the combined action of an AGN and a central starburst, whose presence is indicated by a ring of bright Hα emitting regions in the central part of the galaxy. The X-ray emission from NGC 89 was modelled as that of both an absorbed AGN and a diffuse emission coming from the central starburst (Trinchieri et al. 2008). However, we cannot exclude the possibility of an inflow. To discriminate between an inflow and an outflow beyond any doubt, we would need a detailed study of the interstellar absorption-line profiles, such as those of NaI D $\lambda\lambda$ 5890, 5896 Å (e.g., Rupke et al. 2005a).

Although another possibility is that a minor merger occurred recently and that a dwarf satellite was cannibalised by NGC 89, we find this interpretation less likely. At least with the existing data, we could find no trace of a secondary nucleus in NGC 89. A search of the NED archive for the presence of dwarf satellites around the group found only two galaxies within an Abell radius at a comparable redshift. This suggests that SCG0018-4854 is genuinely isolated. However, we cannot exclude that NGC 89 might have had a dwarf satellite that was disrupted by a merger event. However, in the case of a minor merger we would expect to observe structures such as tidal streams that form loops and shells around the main galaxy or features resembling X-shaped jets, as in the case of other systems that have been explained as the result of the disruption of a dwarf galaxy cannibalized by its more massive companion (e.g., Mrk 315 and NGC 1097; see Ciroi et al. 2005; Higdon & Wallin 2003). The Hα images, instead show a wide distribution of extra-planar gas on both sides of the galaxy disk.

On the other hand, both AGN-driven and starburst-driven winds on the galaxy scale have been observed in other Seyfert 2 and starburst galaxies in both the local Universe and at higher redshifts (see Veilleux et al. 2005, for a review). Powerful large-scale outflows might be caused by strong starburst activity in the central regions of a galaxy with the consequent shock-heating and acceleration of ambient interstellar gas (e.g., Heckman et al. 1990). Simulations of starburst-driven galactic winds find that optically emitting filaments can be formed by fragmentation and acceleration of a cloud into a supersonic wind (Cooper et al. 2008). When radiative cooling is taken into account, these fragments survive to generate strands and filaments downstream of the original cloud position as seen in starburst-driven winds (Cooper et al. 2009). A well known case is that of M 82, which contains optical filaments whose velocities increase with radius

(Shopbell & Bland-Hawthorn 1998). The observed morphologies and kinematics of outflowing gas on large scales is reminescent of the structures that we observed in NGC 89. By analysing a sample of infrared luminous starbursts, Rupke et al. (2005b) found that superwinds are ubiquitous in these galaxies and in most cases the outflowing gas has velocities of 100–200 km s^{-1}.

Bomans et al. (1997), Tschöke et al. (2001), and Strickland et al. (2004) demonstrated that a correlation exists between Hα outflow structures and X-ray features. Cooper et al. (2009) also found that the soft X-ray emission is produced by mass ablated from the clouds and mixed with the surrounding gas. After 0.75 Myr, the fraction of gas mixed into the surrounding gas is $\approx$25%. Hence, we would expect to observe some X-ray features correlated to the galactic-scale filaments of NGC 89. Trinchieri et al. (2008) did not detect any X-ray feature linked to the Hα emission. However, the total number counts of their X-ray observations and the presence of two dominant components in the emission related to NGC 89, namely an absorbed AGN and an unresolved component from binary systems, would make it extremely difficult to detect a additional faint component related to the low surface brightness Hα filaments tracing the extra-planar gas (flux$_{H\alpha}$ = 10^{-16}–10^{-17} erg s^{-1} cm^{-2}). Any interaction of the outflow with the IGM is also expected to be very weak, since the IGM in which the members of SCG0018-4854 are embedded is cooler ($kT \approx 0.2$ keV) and less dense ($n_e \approx 5 \times 10^{-3}$ cm^{-3}) than that typically found in other environments, such as groups with a central elliptical galaxy or the cores of clusters (Trinchieri et al. 2008).

Our study of NGC 89 have found a complex gas kinematics in the inner regions: the galaxy emission-line profiles have multiple components along both the major and the minor axes. We have presented evidence of at least two secondary components along both axes: one blue-shifted and the other red-shifted. This type of composite motion is well known in literature for the NLR of Seyfert galaxies (Das et al. 2006, and references therein). However, a detailed kinematical model for the NLR is beyond the scope of this paper. The presence of a possible fourth component in the emission-line profile along the minor axis is intriguing as this component is visible only in the direction of the galactic-scale extra-planar features. If indeed a galactic-scale outflow is present, we cannot exclude a link between this outflow and the central engine.

In Sect. 5.2, we probed the kinematics of the extra-planar gas at a few positions. The velocity difference of $\approx$60 km s^{-1} between the two measured positions in the NE direction could be indicative of two gas shells with different velocities due to the impact of the gas with the ISM. Moreover, when going far away from the nucleus along the minor axis we found that the gas accelerates in the SW direction, which is consistent with an outflow interpretation.

Therefore, the combined information derived from the kinematics and the geometry of the ionised extraplanar gas favours an outflow scenario. Marquez et al. (1998) studied a similar case: NGC 2992 is a Seyfert 1.9 galaxy with an emission arc, visible in [OIII] and Hα, which is interacting with its companion NGC 2993. A radial outflow was added to the circular motion to account for the observed kinematics. They found that the largest differences with respect to the model were found when going to larger distances from the nucleus and suggested that these are kinematically distinct regions where the gas could be perturbed by the interaction of NGC 2992 with its close companion NGC 2993. This could also be the case for NGC 89 since the HI velocity field implies that the tidal tail of NGC 92 points

towards the observer with a velocity comparable to that of NGC 89 (Pompei et al. 2007)

With the currently available data, we are not able to establish the origin of the galactic-scale outflow. Integral-field spectroscopy would be useful in helping us to understand the outflow kinematics and constrain its origin.

6.4. Comparing SCG0018-4854 with HCG16

The extreme physical properties of SCG0018-4854 make it a very interesting and rare group. It could be considered the southern counterpart of HCG16, the group with the highest concentration of late-type active and interacting galaxies in the nearby universe. Therefore, we compare its kinematic properties with those found in the literature for HCG 16. The latest and most detailed kinematical study of HCG16 was carried out by Mendes de Oliveira et al. (1998) using Fabry-Perot data. They found kinematic peculiarities for three galaxies out of the four originally listed in Hickson's catalogue (Hickson 1982). They found a non-axisymmetric rotation curve with a velocity discrepancy of 100 km s^{-1} between the two sides and a slow rise in the central region. They discovered a second component in the emission-line profile of one galaxy. They detected the severe warping of the kinematic major axis of two galaxies and finally the presence of a double nucleus and a peculiar bar-like structure. Based on these results, they suggested that major merger events have occurred in at least two out of four galaxies. Our study finds that most of these kinematical peculiarities are also present in SCG0018-4854, confirming that it is a relatively dynamically young and active CG.

7. Conclusions

We have analyzed high signal-to-noise spectra along both the major and the minor axis of each member galaxy of SCG0018-4854. Each galaxy has disturbed or peculiar kinematics. Kinematic information is important in obtaining insight into the possible interaction history of the galaxies. Different interaction scenarios, depending on the strength and the geometry of the encounter and the morphological types of the interacting systems, will leave different signatures on the galaxy kinematics. Following Mendes de Oliveira et al. (1998), we found signs of disturbed velocity fields, asymmetric rotation curves, multiple kinematical gas components, tidal tails, and nuclear activity. All of these characteristics suggest that at least three out of four galaxies of SCG0018-4854 have been involved in a strong and recent interaction. We derived some constraints on the age of the latest close interaction: $\approx$190 Myr $< \tau_{coll} < 0.7$ Gyr. The interaction has been strong enough to perturb the gas kinematics up to a level of 24% for the gas of the two main galaxies. These results agree with the recent claim by Torres-Flores et al. (2009) that this group is in an advanced stage of interaction, based on the presence of young star-forming region, a candidate tidal dwarf galaxy identified in the UV, and the observed tidal tails. Finally, the results of our spectroscpic analysis are consistent with the hypothesis of a large-scale outflow in NGC 89.

In contrast to its evolved properties as a group, such as its high spatial density, the spatial distribution of HI, and the presence of a common hot IGM, SCG0018-4854 consists entirely of spiral galaxies and has a remarkably high fraction of active galaxies. This study has found kinematical signs of recent interactions among its members making SCG0018-4854 a dynamically young group, although its global properties are indicative of a more advanced stage of evolution.

Given the estimated age of the latest interaction, we could say that we catch these galaxies in the act of interacting. What about the future of this group? Hydrodynamical simulations could help us to understand the fate of SCG 0018-4854, a true isolated and interacting compact group.

References

Appenzeller, I., Fricke, K., Fürtig, W., et al. 1998, The Messenger, 94, 1
Barnes, J. 1985, MNRAS, 215, 517
Bautista, M. A. 1999, ApJ, 527, 474
Belsole, E., Sauvageot, J.-L., Ponman, T. J., & Bourdin, H. 2003, A&A, 398, 1
Bomans, D. J., Chu, Y.-H., & Hopp, U. 1997, AJ, 113, 1678
Boselli, A., Mendes de Oliveira, C., Balkowski, C., Cayatte, V., & Casoli, F. 1996, A&A, 314, 738
Ciroi, S., Afanasiev, V. L., Moiseev, A. V., et al. 2005, MNRAS, 360, 253
Coccato, L., Corsini, E. M., Pizzella, A., et al. 2004, A&A, 416, 507
Cooper, J. L., Bicknell, G. V., Sutherland, R. S., & Bland-Hawthorn, J. 2008, ApJ, 674, 157
Cooper, J. L., Bicknell, G. V., Sutherland, R. S., & Bland-Hawthorn, J. 2009, ArXiv e-prints
Corsini, E. M., Pizzella, A., Coccato, L., & Bertola, F. 2003, A&A, 408, 873
Coziol, R., & Plauchu-Frayn, I. 2007, AJ, 133, 2630
Coziol, R., Iovino, A., & de Carvalho, R. R. 2000, AJ, 120, 47
Crowther, P. A. 2007, ARA&A, 45, 177
Dale, D. A., Giovanelli, R., Haynes, M. P., Hardy, E., & Campusano, L. E. 2001, AJ, 121, 1886
Danks, A. C., & Alcaino, G. 1981, A&A, 98, 223
Das, V., Crenshaw, D. M., Kraemer, S. B., & Deo, R. P. 2006, AJ, 132, 620
de Carvalho, R. R., & Coziol, R. 1999, AJ, 117, 1657
Díaz, A. I., Castellanos, M., Terlevich, E., & Luisa García-Vargas, M. 2000, MNRAS, 318, 462
Dopita, M. A., Groves, B. A., Sutherland, R. S., Binette, L., & Cecil, G. 2002, ApJ, 572, 753
Fraternali, F., & Binney, J. J. 2008, MNRAS, 386, 935
Gallart, C., Martínez-Delgado, D., Gómez-Flechoso, M. A., & Mateo, M. 2001, AJ, 121, 2572
Gerin, M., Combes, F., & Athanassoula, E. 1990, A&A, 230, 37
Governato, F., Tozzi, P., & Cavaliere, A. 1996, ApJ, 458, 18
Heckman, T. M., Armus, L., & Miley, G. K. 1990, ApJS, 74, 833
Hickson, P. 1982, ApJ, 255, 382
Hickson, P., Mendes de Oliveira, C., Huchra, J. P., & Palumbo, G. G. 1992, ApJ, 399, 353
Higdon, J. L., & Wallin, J. F. 2003, ApJ, 585, 281
Iovino, A. 2000, in Small Galaxy Groups, ed. M. J. Valtonen, & C. Flynn, ASP Conf. Ser., 209, IAU Coll., 174, 25
Keel, W. C. 1993, AJ, 106, 1771
Kraemer, S. B., & Crenshaw, D. M. 2000, ApJ, 544, 763
Kronberger, T., Kapferer, W., Schindler, S., et al. 2006, A&A, 458, 69
Kuijken, K., & Merrifield, M. R. 1995, ApJ, 443, L13
Lindblad, P. O. 1961, Sov. Astron., 5, 376
Marquez, I., Boisson, C., Durret, F., & Petitjean, P. 1998, A&A, 333, 459
Mendes de Oliveira, C., & Hickson, P. 1994, ApJ, 427, 684
Mendes de Oliveira, C., Plana, H., Amram, P., Bolte, M., & Boulesteix, J. 1998, ApJ, 507, 691
Noguchi, M. 1987, MNRAS, 228, 635
Osterbrock, D. E., & Ferland, G. J. 2006, Astrophysics of gaseous nebulae and active galactic nuclei, ed. G. J. Osterbrock, & D. E. Ferland
Osterbrock, D. E., & Mathews, W. G. 1986, ARA&A, 24, 171
Pedrosa, S., Tissera, P. B., Fuentes-Carrera, I., & Mendes de Oliveira, C. 2008, A&A, 484, 299
Pompei, E., Dahlem, M., & Iovino, A. 2007, A&A, 473, 399
Ribeiro, A. L. B., de Carvalho, R. R., Coziol, R., Capelato, H. V., & Zepf, S. E. 1996, ApJ, 463, L5
Roche, N. D. 2007, Rev. Mex. Astron. Astrofis., 43, 179
Rose, J. A. 1977, ApJ, 211, 311
Rubin, V. C., Hunter, D. A., & Ford, W. K. J. 1991, ApJS, 76, 153
Rupke, D. S., Veilleux, S., & Sanders, D. B. 2005a, ApJ, 632, 751
Rupke, D. S., Veilleux, S., & Sanders, D. B. 2005b, ApJS, 160, 115
Schaerer, D., & Vacca, W. D. 1998, ApJ, 497, 618
Shopbell, P. L., & Bland-Hawthorn, J. 1998, ApJ, 493, 129
Strickland, D. K., Heckman, T. M., Colbert, E. J. M., Hoopes, C. G., & Weaver, K. A. 2004, ApJS, 151, 193
Sulentic, J. W. 1987, ApJ, 322, 605
Temporin, S., Ciroi, S., Iovino, A., et al. 2005, Starbursts: From 30 Doradus to Lyman Break Galaxies, ed. R. de Grijs, & R. M. González Delgado, Ap&SS Library, 329, 78P
Tonry, J., & Davis, M. 1979, AJ, 84, 1511
Torres-Flores, S., Mendes de Oliveira, C., de Mello, D. F., et al. 2009, A&A, 507, 723
Trinchieri, G., Iovino, A., Pompei, E., et al. 2008, A&A, 484, 195
Tschöke, D., Bomans, D. J., Hensler, G., & Junkes, N. 2001, A&A, 380, 40
Veilleux, S. 1991, ApJS, 75, 383
Veilleux, S., Cecil, G., & Bland-Hawthorn, J. 2005, ARA&A, 43, 769
Verdes-Montenegro, L., Yun, M. S., Williams, B. A., et al. 2001, A&A, 377, 812